

Non-Abelian symmetry can increase entanglement entropy

Shayan Majidy,^{1,2,*} Aleksander Lasek,³ David A. Huse,⁴ and Nicole Yunger Halpern^{3,5,†}

¹*Institute for Quantum Computing, University of Waterloo, Waterloo, Ontario N2L 3G1, Canada*

²*Perimeter Institute for Theoretical Physics, Waterloo, Ontario N2L 2Y5, Canada*

³*Joint Center for Quantum Information and Computer Science,*

NIST and University of Maryland, College Park, MD 20742, USA

⁴*Department of Physics, Princeton University, Princeton, NJ 08544, USA*

⁵*Institute for Physical Science and Technology, University of Maryland, College Park, MD 20742, USA*

(Dated: September 30, 2022)

The pillars of quantum theory include entanglement and operators’ failure to commute. The Page curve quantifies the bipartite entanglement of a many-body system in a random pure state. This entanglement is known to decrease if one constrains extensive observables that commute with each other (Abelian “charges”). Non-Abelian charges, which fail to commute with each other, are of current interest in quantum thermodynamics. For example, noncommuting charges were shown to reduce entropy-production rates and may enhance finite-size deviations from eigenstate thermalization. Bridging quantum thermodynamics to many-body physics, we quantify the effects of charges’ noncommutation—of a symmetry’s non-Abelian nature—on Page curves. First, we construct two models that are closely analogous but differ in whether their charges commute. We show analytically and numerically that the noncommuting-charge case has more entanglement. Hence charges’ noncommutation can promote entanglement.

Introduction.—Entanglement has illuminated quantum many-body phenomena from space-time’s structure [1–3] to phases [4–12] and thermalization [13]. A large, isolated many-body system thermalizes internally when evolved under a nonintegrable, chaotic Hamiltonian. Such dynamics tend to imbue an initial pure state, after long times, with properties closely approximated in pure states drawn randomly from the available Hilbert space. The random state’s average bipartite entanglement is quantified with a *Page curve* [14]: Consider partitioning the system into two subsystems, calculating a subsystem’s entanglement entropy, and averaging the entropy over states drawn randomly from the full system’s Hilbert space. The average, plotted against the subsystem’s size, forms a Page curve.

Page curves have been studied in the context of Abelian symmetries [15–34]. Consider a many-body system whose evolution conserves an extensive observable, or *charge*; examples include the total particle number. Studying thermalization properties via a Page curve, one draws random pure states from a chosen particle-number sector—an eigenspace of the charge. We call such an eigenspace a *microcanonical* subspace \mathcal{S} . More generally, the system may have multiple charges that commute with each other, so that the symmetry remains Abelian. \mathcal{S} can be chosen to be an eigenspace shared by the charges (apart from the Hamiltonian).

However, noncommutation lies at the heart of quantum theory, underlying uncertainty relations, measurement disturbance, and notions of locality [35, 36]. Conserved charges can fail to commute with each other, though charges’ commutation was assumed implicitly

across thermodynamics for decades [37–44]. The assumption was lifted in quantum thermodynamics recently [39–76]. Noncommuting charges have been shown to invalidate derivations of the thermal state’s form [40, 42]; reduce entropy-production rates [58]; and potentially enhance finite-size corrections to the eigenstate thermalization hypothesis, a framework for explaining quantum systems’ internal thermalization [41]. The experimental testing of these results [49] has begun with a trapped-ion simulator [50]. Inspired by quantum thermodynamics, we aim to quantify a particularly quantum feature of many-body physics in this paper: how charges’ noncommutation—a symmetry’s non-Abelian nature—affects Page curves.

This comparison calls for two models that parallel each other closely, yet differ in whether their charges commute. Whether such models exist, what “parallel closely” should mean, and how to construct such models is unclear. We therefore posit criteria to encapsulate models’ analogousness. Furthermore, we construct two models that meet these criteria. Each model consists of two-qubit sites. Every local charge is a product of two-qubit Pauli operators and/or identity operators.

We compare these models’ Page curves in two settings. Conventional thermodynamics suggests one: a microcanonical subspace, a simultaneous eigenspace of the charges. The noncommuting-charge model has only one microcanonical subspace, because noncommutation tends to block observables from having well-defined values simultaneously. Also, the notion of a microcanonical subspace has been generalized to an *approximate microcanonical (AMC) subspace*, to accommodate noncommuting charges [42, 50, 59]. Here, every charge has a fairly well-defined value: Measuring any charge has a high probability of yielding an outcome close to the expected value. We identify AMC subspaces

* smajidy@uwaterloo.ca

† nicoleyh@umd.edu

in the noncommuting-charge model and analogs in the commuting-charge model. Each pair of such subspaces yields another pair of Page curves.

We estimate the Page curves numerically and, in the microcanonical comparison, analytically. In every setting where we can do so, the noncommuting-charge Page curve lies above the commuting-charge curve. On average, therefore, charges' noncommutation appears to promote entanglement. For systems of $N \gg 1$ sites, the Page curves' separation decreases, but only polynomially in the system size, as $1/N$. We posit that the gap arises solely from whether the charges commute, due to the close parallel between our two models. This conjecture calls for testing with more parallel models and with more-general explanations, which we leave as a challenge for future research.

The rest of this paper is organized as follows. First, we overview Page curves. Then, we present the analogous models. We compare Page curves using microcanonical subspaces, then using AMC subspaces. To conclude, we describe opportunities established by this work.

Page-curve background.—To introduce Page curves, we must introduce entanglement entropy. Consider an isolated (“global”) system, associated with a Hilbert space \mathcal{H} , in a pure state $|\Phi\rangle$. Denote by A a subsystem associated with a dimension- D_A Hilbert space. Denote by B the rest of the system. The full system's Hilbert space is the outer product of the subsystems' Hilbert spaces. The *entanglement entropy* is the von Neumann entropy of $\rho_A := \text{Tr}_B(|\Phi\rangle\langle\Phi|)$ [77]:

$$S_E := S(\rho_A) := -\text{Tr}(\rho_A \log \rho_A) \leq \log D_A. \quad (1)$$

The logarithms are base- e , giving entropies in units of nats. A is entangled with B if $S_E > 0$.

The Page curve quantifies the average entanglement in a subspace \mathcal{S} of interest. Let A consist of N_A identical sites, and let B consist of N_B more, such that $N_A + N_B = N$. Consider selecting a global pure state from \mathcal{S} uniformly randomly—according to the Haar measure [78]. Calculating S_E , then averaging over Haar-random states, yields

$$\langle S_E \rangle_{\mathcal{S}} := -\langle \text{Tr}(\rho_A \log \rho_A) \rangle_{\mathcal{S}}. \quad (2)$$

Plotted against N_A , $\langle S_E \rangle_{\mathcal{S}}$ forms the Page curve for subspace \mathcal{S} [14].

We estimate the curve numerically as follows. Denote by $\{|\psi_\ell\rangle\}$ any basis for the subspace. We weight the ℓ^{th} element with a random number c_ℓ drawn from a complex normal distribution. Summing the weighted elements, and renormalizing with a constant C_{norm} , we form a Haar-random state: $\frac{1}{C_{\text{norm}}} \sum_\ell c_\ell |\psi_\ell\rangle$. We sample 10^3 – 10^4 states, calculate each state's S_E , and average to estimate the Page curve.

In the best-known example, no charges constrain the system [14]. Denote by \mathcal{H} the full Hilbert space and by d the local dimension (of a site's Hilbert space). The

unconstrained Page curve is, for $N_A \leq N_B$,

$$\langle S_E \rangle_{\mathcal{H}} \approx N_A \log d - \frac{1}{2} d^{N_A - N_B}. \quad (3)$$

The terms in Eq. (3) stem from different physics, as do the analogous terms in constrained Page curves. Consider averaging the Haar-random states over \mathcal{S} before calculating any entropy. The averaged state, $\langle \rho \rangle_{\mathcal{S}}$, is the maximally mixed state within \mathcal{S} . Tracing out B yields $\langle \rho_A \rangle_{\mathcal{S}} := \text{Tr}_B(\langle \rho \rangle_{\mathcal{S}})$, whose entropy follows from state-counting arguments (App. A). We therefore call $S(\langle \rho_A \rangle_{\mathcal{S}})$ the subspace- \mathcal{S} Page curve's *state-counting term*. In terms of it, the curve decomposes as

$$\langle S_E \rangle_{\mathcal{S}} = S(\langle \rho_A \rangle_{\mathcal{S}}) + [\langle S_E \rangle_{\mathcal{S}} - S(\langle \rho_A \rangle_{\mathcal{S}})]. \quad (4)$$

Since $\langle \rho \rangle_{\mathcal{S}}$ is maximally mixed, $S(\langle \rho_A \rangle_{\mathcal{S}})$ equals the greatest possible entropy: $\langle S_E \rangle_{\mathcal{S}} \leq S(\langle \rho_A \rangle_{\mathcal{S}})$. Hence the bracketed term in Eq. (4) is ≤ 0 . That term encodes the interference between different states' contributions to the Page curve's Haar average. This *interference term* is exponentially small in $N_B - N_A$ [14]. In the unconstrained curve (3), $N_A \log d$ is the state-counting term, and $-\frac{1}{2}d^{N_A - N_B}$ is the interference term.

Analogous noncommuting-charge and commuting-charge models.—We aim to identify how charges' noncommutation affects the Page curve. Therefore, we need two models that differ in whether their charges commute and otherwise differ minimally. Whether such models exist, what “differ minimally” should mean, and how to construct such models is unclear. For instance, the most commonly studied non-Abelian symmetry group is $\text{SU}(2)$; the associated charges are the Pauli operators X , Y , and Z . How to construct an analogous model with three commuting charges is not obvious. The group $\text{U}(1)^{\times 3}$ is generated by three charges that commute but are not multiplicatively interrelated. In contrast, $XY = iZ$.

We address this challenge by positing five criteria that capture what renders noncommuting-charge and commuting-charge models analogous. Then, we construct two models that meet these criteria. We denote by Q_α^{tot} the global noncommuting charges and by C_α^{tot} the global commuting charges. The criteria also concern the subspaces used to calculate the Page curves. Denote by $|\psi\rangle$ any state from the noncommuting-charge subspace \mathcal{N} . Measuring Q_α^{tot} yields outcome γ with some probability. This probability, averaged over the $|\psi\rangle$, we denote by $p_\alpha^{\mathcal{N}}(\gamma)$. Define $p_\alpha^{\mathcal{C}}(\gamma)$ analogously for the commuting-charge subspace \mathcal{C} .

We define as analogous commuting-charge and noncommuting-charge models that satisfy five criteria:

1. In each model, the system consists of N sites, each formed from a d -level qudit. Each model has c constrained global charges.
2. Each global charge is a sum of single-site observables. Furthermore, each global charge acts nontrivially and identically on all sites.

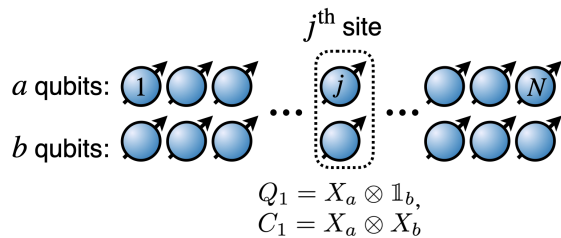


Figure 1: Analogous noncommuting-charge and commuting-charge models. Each model consists of N sites. A site consists of two qubits, a and b . The local noncommuting observables of interest include Q_1 ; and the local commuting observables, C_1 .

3. Each charge Q_α^{tot} has the same spectrum as its analog C_α^{tot} .
4. The commuting charges generate an algebra whose structure constants closely resemble the noncommuting-charge algebra's structure constants [49].
5. The constrained subspaces, \mathcal{N} and \mathcal{C} , are such that $p_\alpha^{\mathcal{N}}(\gamma) = p_\alpha^{\mathcal{C}}(\gamma)$.

We now construct models that satisfy the criteria (Fig. 1). Each global charge (Q_α^{tot} or C_α^{tot}) follows from summing single-site observables Q_α or C_α . Denote by $Q_\alpha^{(j)}$ an observable defined on site j 's Hilbert space, and define $C_\alpha^{(j)}$ analogously. The global charges are extensive: If $\mathbb{1}$ denotes the single-site identity operator,

$$Q_\alpha^{\text{tot}} := \sum_{j=1}^N \mathbb{1}^{\otimes(j-1)} \otimes Q_\alpha^{(j)} \otimes \mathbb{1}^{\otimes(N-j)} \equiv \sum_{j=1}^N Q_\alpha^{(j)}, \quad (5)$$

and $C_\alpha^{\text{tot}} := \sum_{j=1}^N C_\alpha^{(j)}$.

The noncommuting charges can generate $\mathfrak{su}(2)$ if each site contains one qubit ($d = 2$). By criterion 2, three charges impose three restrictions on each site. A fourth restriction follows from the normalization of the site's state. These restrictions suggest that, to support a model with three commuting charges, d should be ≥ 4 . Choosing $d = 4$ for simplicity, we form each site's qudit from two qubits, a and b . The noncommuting local observables are

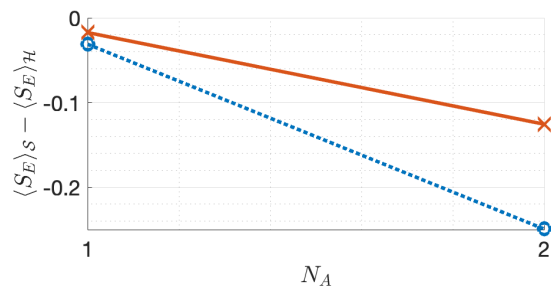
$$Q_1 = X_a \otimes \mathbb{1}_b, \quad Q_2 = Y_a \otimes \mathbb{1}_b, \quad \text{and} \quad Q_3 = Z_a \otimes \mathbb{1}_b; \quad (6)$$

and the commuting local observables are

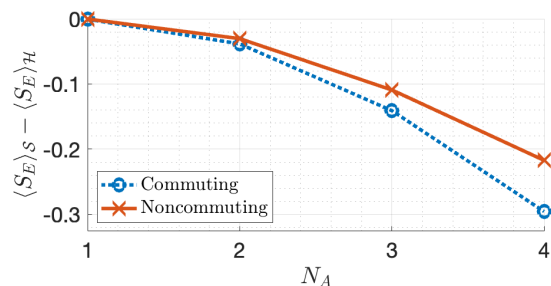
$$C_1 = X_a \otimes X_b, \quad C_2 = Y_a \otimes Y_b, \quad \text{and} \quad C_3 = Z_a \otimes Z_b. \quad (7)$$

These models satisfy criteria 1–3 overtly and by simple calculation. Criterion 4 concerns the structure constants. For unequal indices $\alpha, \beta, \gamma \in \{1, 2, 3\}$,

$$Q_\alpha Q_\beta = i\epsilon_{\alpha\beta\gamma} Q_\gamma, \quad \text{and} \quad C_\alpha C_\beta = -C_\gamma. \quad (8)$$



(a) Global-system size $N = 4$



(b) Global-system size $N = 8$

Figure 2: Page curves constructed from microcanonical subspaces. $\langle S_E \rangle_{\mathcal{S}}$ denotes any Page curve restricted by charges; and $\langle S_E \rangle_{\mathcal{H}}$, the unrestricted Page curve. The red x's form the noncommuting-charge model's Page curve, and the circular blue markers form the commuting-charge model's Page curve. The connecting lines guide the eye. We calculated the top panel's ($N = 4$) Page curves from 10^4 samples each and the bottom panel's ($N = 8$) Page curves from 10^3 samples each. The x -axis ends at $N_A = N/2$ for conciseness; the Page curves are symmetric according to numerics.

These equations parallel each other because multiplying two distinct charges yields the third charge times a constant. Furthermore, $Q_\alpha Q_\alpha = C_\alpha C_\alpha = \mathbb{1}$ for each α .

Criterion 5 is satisfied if we choose subspaces adroitly. In the microcanonical subspaces identified below, the $p_\alpha^{\mathcal{N}}(\gamma)$'s and $p_\alpha^{\mathcal{C}}(\gamma)$'s equal each other and Kronecker delta functions. As detailed below, we can also construct AMC subspaces such that $p_\alpha^{\mathcal{N}}(\gamma) = p_\alpha^{\mathcal{C}}(\gamma)$ for all α and γ .

Microcanonical-subspace comparison.—The noncommuting-charge model has exactly one microcanonical subspace, \mathcal{N}_0 : the eigenvalue-0 eigenspace shared by $Q_{1,2,3}^{\text{tot}}$. This subspace exists only if N is even. The analogous commuting-charge subspace, \mathcal{C}_0 , is the eigenvalue-0 eigenspace shared by $C_{1,2,3}^{\text{tot}}$. This subspace exists only if N equals a multiple of four (App. A 2).

We estimate Page curves numerically using the procedure outlined in “Page-curve background” above. Here, $\langle S_E \rangle_{\mathcal{S}}$ denotes the Page curve for a subspace \mathcal{S} , and $\langle S_E \rangle_{\mathcal{H}}$ denotes the unrestricted Page curve (3). To highlight the gap between the noncommuting-charge and commuting-charge curves, we plot $\langle S_E \rangle_{\mathcal{S}} - \langle S_E \rangle_{\mathcal{H}}$ for $\mathcal{S} = \mathcal{N}_0, \mathcal{C}_0$ in Fig. 2. At all partition locations N_A , the noncommuting-charge Page curve lies above the

commuting-charge Page curve. For example, at the midpoint ($N_A = N/2$), the gap is 0.124 nats (17.8% of the average of the two Page curves at $N_A = N/2$) when $N = 4$ and 0.0797 nats (10.5%) when $N = 8$. In this microcanonical case, therefore, the subspace constrained by noncommuting charges has more entanglement, on average.

We posit the following explanation for this phenomenon in our setting. The commuting-charge model's microcanonical subspace, \mathcal{C}_0 , has a tensor-product basis. The reason is, every global charge C_{α}^{tot} commutes with all the subsystem charges $C_{\alpha'}^{(A)}$ and $C_{\alpha''}^{(B)}$. In contrast, in the noncommuting-charge model, each global charge Q_{α}^{tot} fails to commute with some subsystem charges $Q_{\alpha'}^{(A)}$ and $Q_{\alpha''}^{(B)}$. Hence the microcanonical subspace \mathcal{N}_0 has no tensor-product basis. Therefore, the minimally entangled basis has more entanglement in the noncommuting-charge model. Hence one might expect a higher Page curve there. We also quantify, in App. C, to what extent introducing the charges sequentially alters the Page curve additively.

We now analytically estimate the difference between the noncommuting-charge and commuting-charge Page curves in these microcanonical subspaces at large N . Recall that the interference term [Eq. (4)] is exponentially small in $N_B - N_A$ [14]. Consequently, the Page curve approximately equals the state-counting term when $N_B - N_A \gg 1$ [79]. We estimate state-counting terms in App. A, using large- N expansions. We assume that $N_A, N_B = \mathcal{O}(N)$; the subsystems' sizes are near their average values. Both subspaces' Page curves have the leading, $\mathcal{O}(N^0)$ term

$$L := N_A \log d - \frac{3}{2} \log \frac{N}{N_B} + \frac{3N_A}{2N}. \quad (9)$$

The noncommuting-charge Page curve is

$$L + \frac{3N_A}{4N^2} + \frac{N_A^2}{2N^2N_B} + \mathcal{O}\left(N^{-\frac{3}{2}}\right), \quad (10)$$

and the commuting-charge Page curve is [80]

$$L + \frac{3N_A}{4N^2} - \frac{N_A^2}{2N^2N_B} + \mathcal{O}\left(N^{-\frac{3}{2}}\right). \quad (11)$$

The noncommuting-charge Page curve is greater by an amount $\frac{N_A^2}{N^2N_B}$, at leading order. The difference decreases as N grows. This decline is consistent with the correspondence principle [81]—as systems grow large, they grow classical. Noncommutation is nonclassical, so its effects on observable phenomena should diminish as $N \rightarrow \infty$ [42]. More precisely, the charge densities $Q_{\alpha}^{\text{tot}}/N$ have commutators that vanish in the thermodynamic limit [42, 82]: $[Q_{\alpha}^{\text{tot}}/N, Q_{\alpha'}^{\text{tot}}/N] \rightarrow 0$, for all α and α' , as $N \rightarrow \infty$. However, the Page-curve difference shrinks relatively slowly—as $\sim 1/N$, rather than exponentially, as N grows.

Approximate-microcanonical-subspace comparison.— Having compared our two models using microcanonical subspaces, we progress to AMC subspaces, generalizations that accommodate charge noncommutation [42, 50, 59]. Instead of having well-defined values in an AMC subspace, the charges have fairly well-defined values: Measuring any Q_{α}^{tot} has a high probability of yielding an outcome close to the expected value. In this section, we explain how to construct analogous AMC subspaces in the noncommuting-charge and commuting-charge models. We then compare the models' Page curves numerically. The noncommuting-charge Page curve is always higher, as in the microcanonical-subspace comparison.

One can construct as follows AMC subspaces in the noncommuting-charge model. Denote by $2m$ the Z_a^{tot} eigenvalue. Define the a -type spin-squared operator $(\tilde{S}_a^{\text{tot}})^2 := \sum_{a=1}^3 (Q_a^{\text{tot}})^2$, which has eigenvalues $s(s+1)$ (we set $\hbar = 1$). $(\tilde{S}_a^{\text{tot}})^2$ shares with Z_a^{tot} —and so $(\tilde{S}_a^{\text{tot}})^2 \otimes \mathbb{1}_b^{\text{tot}}$ shares with Q_3^{tot} —eigenspaces \mathcal{N} labeled by the quantum numbers (s, m) . Some such eigenspaces are AMC subspaces, we find by direct calculation. For each (s, m) value, we calculate the probability distributions $p_{\alpha}^{\mathcal{N}}(\gamma)$. Each distribution exhibits one peak, as required by the definition of ‘‘AMC subspace,’’ for certain (s, m) (App. D). Having identified AMC subspaces defined by noncommuting charges, we construct analogs \mathcal{C} defined by commuting charges. Appendix D details the process. We identify six pairs of parallel (commuting-charge and noncommuting-charge) AMC subspaces, labeled by $s = m = 1, N/2$, for $N = 4, 8$, as well as by $s = m = N/2$, for $N = 2, 6$.

We estimate each AMC subspace's Page curve numerically. In every comparison, the noncommuting-charge (\mathcal{N}) Page curve lies above its commuting-charge (\mathcal{C}) partner. An illustrative example is parameterized by $N = 8$ and $s = m = 1$. We compare the two curves at the midpoint $N_A = N/2$. Recall that $\langle S_E \rangle_{\mathcal{S}}$ denotes a Page curve for the subspace \mathcal{S} . When $N_A = 4$, $\langle S_E \rangle_{\mathcal{N}} - \langle S_E \rangle_{\mathcal{C}} = 0.027$ nats, which is 7.11% of the two Page curves' average. The percent difference varies across the AMC-subspace pairs from 0.272% to 7.11%. Hence charges' noncommutation increases the average entanglement entropy in AMC subspaces as in the microcanonical comparison.

Outlook.—We have demonstrated that constrained charges' noncommutation promotes entanglement, on average. Numerical and analytical calculations support this conclusion in microcanonical and AMC subspaces. This work reveals how one hallmark of quantum theory—operators' failure to commute—influences another—entanglement.

This conclusion rests on two models that resemble each other closely but differ in whether their charges commute. Our models can now be used to explore effects of charges' noncommutation on other quantum phenomena. Possibilities include chaos [83, 84], as analyzed with out-of-time-ordered correlators [85–88] and random unitary circuits [89, 90]; bounds on quantum-simulation er-

rors [91]; and quantum-machine-learning algorithms’ performances [92].

Additionally, our results raise a puzzle. We find that charges’ noncommutation promotes entanglement, which accompanies thermalization. Another result links noncommuting charges to enhanced thermalization: Non-Abelian symmetries destabilize many-body localization, a phase of matter in which entanglement spreads very slowly [93]. In contrast, charges’ noncommutation was found to restrict thermalizing behaviors in two other settings. First, local observables’ time-averaged expectation values can deviate from thermal predictions by anomalously large corrections, under a physically reasonable assumption, if charges fail to commute [41]. Second, charges’ noncommutation can decrease the rate of entropy production, which accompanies thermalization [48]. These two results technically do not conflict with ours or with Ref. [93], concerning different setups. However, they invite a more general understanding of when non-Abelian symmetries enhance or suppress en-

tanglement and thermalization.

Apart from the foregoing theoretical opportunities, the difference between commuting-charge and noncommuting-charge Page curves may be observed experimentally. For example, at the curves’ midpoints ($N_A = N/2$), the difference is 0.124 nats in the microcanonical setting for $N = 4$, so a precision of ≈ 0.05 nats should suffice to observe the difference. Such a precision has been achieved with trapped ions [94–96] and ultra-cold atoms [97–99]. Furthermore, noncommuting-charge thermodynamics has been argued and demonstrated to be observable on these platforms [49, 50, 59].

Acknowledgements.—We thank Alex Altland, Hubert de Guise, Rajibul Islam, Nathaniel Johnston, Eduardo Martin-Martinez, Tobias Micklitz and Iosif Pinelis for helpful discussions and/or collaborations. This work received support from the National Science Foundation (QLCI grant OMA-2120757). N.Y.H. thanks Princeton, and S.M. thanks QuICS, for their hospitality during the formation of this paper.

Appendix A ANALYTIC EXPRESSIONS FOR STATE-COUNTING TERMS IN MICROCANONICAL SUBSPACES’ PAGE CURVES

The Page curve (2) naturally splits into two terms, the state-counting term [$S(\langle\rho_A\rangle_{\mathcal{S}})$ from Eq. (4)] and the interference term. The interference term is exponentially small in $N_B - N_A$. Thus, if $N_A \ll N_B$, the Page curve approximately equals the state-counting term.

As explained in the main text’s “Page-curve background” section, the state-counting term is easier to calculate than the Page curve is. Consider a system restricted to a subspace \mathcal{S} (e.g., a microcanonical or an AMC subspace) of dimension D . Denote by $\{|\psi_\ell\rangle\}$ any orthonormal basis for the subspace. Taking any pure state from that subspace and Haar-averaging it yields the maximally mixed state, $\langle\rho\rangle_{\mathcal{S}} = \frac{1}{D} \sum_\ell^D |\psi_\ell\rangle\langle\psi_\ell|$. Tracing out B yields $\langle\rho_A\rangle_{\mathcal{S}} := \text{Tr}_B(\langle\rho\rangle_{\mathcal{S}})$, whose entropy is the state-counting term:

$$S(\langle\rho_A\rangle_{\mathcal{S}}) = -\text{Tr}(\langle\rho_A\rangle_{\mathcal{S}} \log \langle\rho_A\rangle_{\mathcal{S}}). \quad (\text{A1})$$

We calculate this term for microcanonical subspaces below. First, we introduce notation, a technical tool, and assumptions (App. A 1). We address the commuting-charge model in App. A 2 and the noncommuting-charge model in App. A 3.

A 1 Preliminaries

We use the following notation throughout this appendix. Denote by $X_a^{\text{tot}} := \sum_{j=1}^N X_a$ the sum of the a qubits’ X operators, and define Y_a^{tot} and Z_a^{tot} analogously. The a qubits’ total-spin-squared operator, $\vec{S}_a^2 = [(X_a^{\text{tot}})^2 + (Y_a^{\text{tot}})^2 + (Z_a^{\text{tot}})^2]/4$, has eigenvalues $s(s+1)$ (we set $\hbar = 1$). Denote by m the $Z_a^{\text{tot}}/2$ eigenvalue. Denote by s_A subsystem A ’s spin quantum number, and denote by m_A subsystem A ’s magnetic spin quantum number. Define s_B and m_B analogously.

We will use Catalan’s triangle, a triangular array of numbers related to the dimensionalities of the Hilbert spaces associated with qubit systems [100, 101]. The element in row a and column b is

$$C_{a,b} = \frac{a-b+1}{a+1} \binom{a+b}{b}, \quad \text{for } a \geq b. \quad (\text{A2})$$

The bound $a \geq b$ lends the array its triangular shape. Temporarily consider an N -qubit system that has quantum numbers s and m . $C_{\frac{N}{2}+s, \frac{N}{2}-s}$ equals the s eigenspace’s dimensionality, for a fixed m .

Throughout our approximations, we assume that parameters approximately equal their typical values: $m, s, m_A, s_A, m_B, s_B = \mathcal{O}(N^{-1/2})$; and $N_A, N_B = \mathcal{O}(N)$. We assume also that the global system is large: $N \gg 1$.

A 2 Commuting-charge model's state-counting term

Appendix A 2 i describes how the commuting-charge model is constrained when in a microcanonical subspace. In App. A 2 ii, we calculate the commuting-charge state-counting term exactly. How the exact formula scales with N is unclear. Therefore, we approximate the term to $\mathcal{O}(N^{-1})$ in App. A 2 iii, to identify differences from the noncommuting-charge model.

A 2 i Constraints on commuting-charge model in microcanonical subspace

The microcanonical subspace \mathcal{C}_0 parallels the noncommuting-charge model's $s = m = 0$ subspace. Let us specify quantitatively how the commuting-charge model is constrained. First, we introduce notation.

The local charges $C_{1,2,3}$ share four eigenstates, the maximally entangled *Bell states* [102]. They are, if $|\uparrow\rangle$ and $|\downarrow\rangle$ denote the Z eigenstates,

$$|B_1\rangle := \frac{1}{\sqrt{2}} (|\downarrow\rangle_a |\uparrow\rangle_b - |\uparrow\rangle_a |\downarrow\rangle_b), \quad |B_2\rangle := \frac{1}{\sqrt{2}} (|\downarrow\rangle_a |\downarrow\rangle_b - |\uparrow\rangle_a |\uparrow\rangle_b), \quad (A3)$$

$$|B_3\rangle := \frac{1}{\sqrt{2}} (|\downarrow\rangle_a |\downarrow\rangle_b + |\uparrow\rangle_a |\uparrow\rangle_b), \quad \text{and} \quad |B_4\rangle := \frac{1}{\sqrt{2}} (|\downarrow\rangle_a |\uparrow\rangle_b + |\uparrow\rangle_a |\downarrow\rangle_b). \quad (A4)$$

The Bell states correspond to the (C_1, C_2, C_3) eigenvalues $(-1, -1, -1)$, $(-1, 1, 1)$, $(1, -1, 1)$, and $(1, 1, -1)$, respectively. We will use a \mathcal{C}_0 basis formed from tensor products of single-site Bell states. For a given basis state, let P_k denote the number of sites in Bell state k .

Having specified notation, we use it to derive constraints on the system. The microcanonical subspace \mathcal{C}_0 is the eigenvalue-0 eigenspace of $C_{1,2,3}^{\text{tot}}$, by analogy with the noncommuting-charge $s = 0$ subspace. If the global system is in an eigenvalue-0 eigenstate of C_1^{tot} , then $P_1 + P_2 = P_3 + P_4 = \frac{N}{2}$. If the system is in an eigenvalue-0 eigenstate of C_2^{tot} , then $P_1 + P_3 = P_2 + P_4 = \frac{N}{2}$. If the system is in an eigenvalue-0 eigenstate of C_3^{tot} , then $P_1 + P_4 = P_2 + P_3 = \frac{N}{2}$. Together, these constraints imply

$$P_1 = P_2 = P_3 = P_4 = N/4. \quad (A5)$$

Since N is an integer, these constraints can be met if N is a multiple of 4, which we assume.

A 2 ii Exact expression for the commuting-charge state-counting term

We first calculate $\langle \rho_A \rangle_{\mathcal{C}_0}$, the reduced state of system A when the global system is maximally mixed. In addition to the definitions above, we invoke the ‘‘quadnomial’’ coefficient $\binom{n}{k_1, k_2, k_3, k_4} := \frac{n!}{k_1! k_2! k_3! k_4!}$. Under the population restriction (A5), the global system's Hilbert space is of dimensionality

$$D = \binom{N}{\frac{N}{4}, \frac{N}{4}, \frac{N}{4}, \frac{N}{4}}. \quad (A6)$$

When subsystem A has populations A_1, A_2, A_3 , and A_4 , the global system is restricted to a subspace of dimensionality

$$\begin{aligned} D_A &= \binom{N_A}{A_1, A_2, A_3, A_4} \binom{N_B}{B_1, B_2, B_3, B_4} \\ &= \binom{N_A}{\frac{N_A}{4} + m_1, \frac{N_A}{4} + m_2, \frac{N_A}{4} + m_3, \frac{N_A}{4} + m_4} \binom{N_B}{\frac{N_B}{4} - m_1, \frac{N_B}{4} - m_2, \frac{N_B}{4} - m_3, \frac{N_B}{4} - m_4}. \end{aligned} \quad (A7)$$

In accordance with Eq. (A5), $A_k + B_k = N/4$. Furthermore, when subsystem A has populations A_1, A_2, A_3 , and A_4 , A is restricted to a subspace of dimensionality

$$d_A = \binom{N_A}{A_1, A_2, A_3, A_4} = \binom{N_A}{\frac{N_A}{4} + m_1, \frac{N_A}{4} + m_2, \frac{N_A}{4} + m_3, \frac{N_A}{4} + m_4}. \quad (A8)$$

The global maximally mixed state is $\langle \rho \rangle_{\mathcal{C}_0} = \frac{1}{D} \sum_{\ell=1}^D |\psi_\ell\rangle\langle\psi_\ell|$; the sum runs over all the states in our basis for \mathcal{C}_0 . Denote by $\{|A_1, A_2, A_3, A_4, i\rangle\}$ a basis for subsystem A 's Hilbert space. The index i distinguishes between basis states that share the same A_1, A_2, A_3 , and A_4 . Tracing out subsystem B yields

$$\langle \rho_A \rangle_{\mathcal{C}_0} = \frac{1}{D} \sum_{A_1, A_2, A_3, A_4, i} \frac{D_A}{d_A} |A_1, A_2, A_3, A_4, i\rangle\langle A_1, A_2, A_3, A_4, i|. \quad (\text{A9})$$

The $\frac{D_A}{d_A}$ equals the dimensionality of the subsystem- B subspace that is consistent with A_1, A_2, A_3 , and A_4 . Taking the spectral decomposition, we calculate $\langle \rho_A \rangle_{\mathcal{C}_0}$'s entropy and so the state-counting term:

$$S(\langle \rho_A \rangle_{\mathcal{C}_0}) = - \sum_{A_1, A_2, A_3, A_4} \frac{D_A}{D} \log\left(\frac{D_A}{d_A D}\right) \quad (\text{A10})$$

$$= - \sum_{A_1, A_2, A_3, A_4} \binom{N_A}{A_1, A_2, A_3, A_4} \frac{\binom{N_B}{B_1, B_2, B_3, B_4}}{\binom{N}{\frac{N}{4}, \frac{N}{4}, \frac{N}{4}, \frac{N}{4}}} \log\left(\frac{\binom{N_B}{B_1, B_2, B_3, B_4}}{\binom{N}{\frac{N}{4}, \frac{N}{4}, \frac{N}{4}, \frac{N}{4}}}\right). \quad (\text{A11})$$

A 2 iii Closed-form approximation to the commuting-charge state-counting term

Let us approximate the $\frac{D_A}{D}$ in Eq. (A10) as a Gaussian function. Via differentiation, we determine that $\log\left(\frac{D_A}{D}\right)$ maximizes at $m_k = 0$ for all k . We Taylor-expand $\log\left(\frac{D_A}{D}\right)$ around this maximum, keeping only terms larger than $\mathcal{O}(N^{-3/2})$. For conciseness, we define $c := \frac{2N}{N_A N_B} = \mathcal{O}\left(\frac{1}{N}\right)$, $d := \frac{1}{3} \left(\frac{8}{N_B^2} - \frac{8}{N_A^2}\right) = \mathcal{O}\left(\frac{1}{N^2}\right)$, $f := \frac{1}{2} \left(\frac{8}{N_A^2} + \frac{8}{N_B^2}\right) = \mathcal{O}\left(\frac{1}{N^2}\right)$, and $g := \frac{1}{2} \left(\frac{32}{3N_A^3} + \frac{32}{3N_B^3}\right) = \mathcal{O}\left(\frac{1}{N^3}\right)$. We substitute these definitions into the expansion of $\log\left(\frac{D_A}{D}\right)$:

$$\begin{aligned} \log\left(\frac{D_A}{D}\right) &= \log\left(\frac{2c^{3/2}}{\pi^{3/2}}\right) - c \left(\sum_{i=1}^4 m_i^2\right) - d \left(\sum_{i=1}^4 m_i^3\right) + f \left(\sum_{i=1}^4 m_i^2\right) - g \left(\sum_{i=1}^4 m_i^4\right) + \frac{5}{4N} - \frac{5}{4N_A} - \frac{5}{4N_B} \\ &+ \mathcal{O}\left(N^{-3/2}\right). \end{aligned} \quad (\text{A12})$$

Exponentiating each side yields

$$\begin{aligned} \frac{D_A}{D} &= 2 \left(\frac{c}{\pi}\right)^{\frac{3}{2}} \exp\left(-c \sum_{i=1}^4 m_i^2\right) \left[1 - d \left(\sum_{i=1}^4 m_i^3\right) + \frac{d^2}{2} \left(\sum_{i=1}^4 m_i^3\right)^2 + f \left(\sum_{i=1}^4 m_i^2\right) - g \left(\sum_{i=1}^4 m_i^4\right) + \frac{5}{4N} - \frac{5}{4N_A} \right. \\ &\left. - \frac{5}{4N_B} + \mathcal{O}\left(N^{-3/2}\right)\right]. \end{aligned} \quad (\text{A13})$$

We check that this function is normalized, as $\frac{D_A}{D}$ should be, but omit the check from this appendix.

Having approximated the first factor in the state-counting term (A10), we address the second, $\log\left(\frac{D_A}{d_A D}\right)$. By Stirling's approximation (A14),

$$\log(n) = n \log(n) - n + \frac{1}{2} \log(2\pi n) + \frac{1}{12n} + \mathcal{O}(n^{-2}), \quad (\text{A14})$$

the logarithm is

$$\begin{aligned} \log\left(\frac{D_A}{d_A D}\right) &= -N \log(4) + \frac{N_B}{4} \log\left(\frac{N_B^4}{\left(\frac{N_B}{4} - m_1\right) \left(\frac{N_B}{4} - m_2\right) \left(\frac{N_B}{4} - m_3\right) \left(\frac{N_B}{4} - m_4\right)}\right) \\ &+ m_1 \log\left(\frac{N_B}{4} - m_1\right) + m_2 \log\left(\frac{N_B}{4} - m_2\right) + m_3 \log\left(\frac{N_B}{4} - m_3\right) + m_4 \log\left(\frac{N_B}{4} - m_4\right) \\ &+ \frac{1}{2} \log\left(\frac{N_B \left(\frac{N}{4}\right)^4}{N \left(\frac{N_B}{4} - m_1\right) \left(\frac{N_B}{4} - m_2\right) \left(\frac{N_B}{4} - m_3\right) \left(\frac{N_B}{4} - m_4\right)}\right) + \frac{5}{4N} + \frac{1}{12N_B} - \frac{1}{12\left(\frac{N_B}{4} - m_1\right)} \\ &- \frac{1}{12\left(\frac{N_B}{4} - m_2\right)} - \frac{1}{12\left(\frac{N_B}{4} - m_3\right)} - \frac{1}{12\left(\frac{N_B}{4} - m_4\right)} + \mathcal{O}\left(N^{-3/2}\right). \end{aligned} \quad (\text{A15})$$

We Taylor-approximate about $N = \infty$ and reorganize:

$$\log\left(\frac{D_A}{d_A D}\right) = -N_A \log(4) + \frac{3}{2} \log\left(\frac{N}{N_B}\right) + \sum_i \left(-\frac{2m_i^2}{N_B} - \frac{8m_i^3}{3N_B^2} + \frac{4m_i^2}{N_B^2} - \frac{16m_i^4}{3N_B^3}\right) + \frac{5}{4N} - \frac{5}{4N_B} + \mathcal{O}\left(N^{-3/2}\right). \quad (\text{A16})$$

The logarithm approximation (A13) and the ratio approximation (A16) can now be substituted into the state-counting term (A10). The summand varies slowly where its value is large, so we approximate the sum as an integral. Also, the integrand falls off quickly enough at large $|A_k|$ that we approximate the limits as $\pm\infty$. Evaluating the resulting Gaussian integrals, we obtain the commuting-charge state-counting term:

$$S(\langle\rho_A\rangle_{C_0}) = N_A \log(4) - \frac{3}{2} \log\left(\frac{N}{N_B}\right) + \frac{3N_A}{N} + \frac{3N_A}{4N^2} - \frac{N_A^2}{2N^2 N_B} + \mathcal{O}\left(N^{-3/2}\right). \quad (\text{A17})$$

A 3 Noncommuting-charge model's state-counting term

The noncommuting charges share exactly one eigenspace, \mathcal{N}_0 , specified as follows. Recall that the a qubits' total-spin-squared operator, \vec{S}_a^2 , has eigenvalues $s(s+1)$. Consider tensoring the a qubits' $s=0$ eigenspace onto the b qubits' full Hilbert space. The product is the eigenvalue-0 eigenspace shared by $Q_{1,2,3}^{\text{tot}}$.

We calculate first the a qubits' contribution to the state-counting term, then the b qubits' contribution (App. A 3 i). In App. A 3 ii, we approximate the state-counting term to order $\mathcal{O}(N^{-1})$, as is necessary for identifying differences from the commuting-charge model.

A 3 i Exact expression for the noncommuting-charge model's state-counting term

First, we calculate the a qubits' contribution to the state-counting term. By the rules for angular-momentum addition, $s = |s_A - s_B|, |s_A - s_B| + 1, \dots, s_A + s_B$. Therefore, $s = m = 0$ only if $|s_A - s_B| = 0$ —equivalently, only if $s_A = s_B$ and $m_A = -m_B$. This restriction constrains the global system to a subspace \mathcal{N}_0 of dimensionality

$$D = C_{\frac{N}{2}, \frac{N}{2}} = \frac{1}{\frac{N}{2} + 1} \binom{N}{\frac{N}{2}}. \quad (\text{A18})$$

We now choose a basis for this subspace. A natural choice consists of states with quantum numbers $s_A = s_B$. If $s_A = s_B = 0$, these basis states are tensor products. However, almost all the basis states correspond to $s_A = s_B > 0$ and encode entanglement between A and B , unlike the basis states chosen for the commuting-charge model. The noncommuting-charge basis states Schmidt-decompose as

$$|s_A, i, j\rangle = \sum_{m_A = -s_A}^{s_A} \frac{(-1)^{m_A}}{\sqrt{2s_A + 1}} |s_A, m_A, i\rangle_A |s_B = s_A, m_B = -m_A, j\rangle_B. \quad (\text{A19})$$

The i indexes the elements of an arbitrary orthonormal basis for the subsystem- A subspace associated with the quantum numbers s_A and m_A . This subspace is of dimensionality

$$d_A = C_{\frac{N_A}{2} + s_A, \frac{N_A}{2} - s_A} = \frac{2s_A + 1}{\frac{N_A}{2} + s_A + 1} \binom{N_A}{\frac{N_A}{2} - s_A}. \quad (\text{A20})$$

The j in (A19) indexes the elements of an arbitrary orthonormal basis for the subsystem- B subspace associated with the quantum numbers s_B and m_B . This subspace is of dimensionality

$$d_B = C_{\frac{N_B}{2} + s_B, \frac{N_B}{2} - s_B} = \frac{2s_B + 1}{\frac{N_B}{2} + s_B + 1} \binom{N_B}{\frac{N_B}{2} - s_B}. \quad (\text{A21})$$

The global system's maximally mixed state is

$$\langle\rho\rangle_{\mathcal{N}_0} = \frac{1}{D} \sum_{s_A, i, j} |s_A, i, j\rangle \langle s_A, i, j|. \quad (\text{A22})$$

Tracing out subsystem B yields

$$\langle \rho_A \rangle_{\mathcal{N}_0} = \frac{1}{D} \sum_{s_A, m_A, i} \frac{d_B}{2s_A + 1} |s_A, m_A, i\rangle \langle s_A, m_A, i|. \quad (\text{A23})$$

Taking the spectral decomposition, we calculate the state's entropy and so the a qubits' contribution to the state-counting term:

$$\begin{aligned} S(\langle \rho_A \rangle_{\mathcal{N}_0}) &= - \sum_{s_A=0}^{\frac{N_A}{2}} \frac{d_A d_B}{D} \log \left(\frac{d_B}{D(2s_A + 1)} \right) \\ &= - \sum_{s_A=0}^{\frac{N_A}{2}} \left(\frac{N}{2} + 1 \right) \frac{(\frac{N}{2})! (\frac{N}{2})!}{N!} \binom{2s_A + 1}{\frac{N_A}{2} + s_A + 1} \binom{2s_A + 1}{\frac{N_B}{2} + s_A + 1} \binom{N_A}{\frac{N_A}{2} - s_A} \binom{N_B}{\frac{N_B}{2} - s_A} \\ &\quad \times \log \left(\frac{(\frac{N}{2})! (\frac{N}{2})!}{N!} \frac{(\frac{N}{2} + 1)}{(\frac{N_B}{2} + s_A + 1)} \binom{N_B}{\frac{N_B}{2} - s_A} \right). \end{aligned} \quad (\text{A24})$$

$$(\text{A25})$$

We now calculate the b qubits' contribution. N_A unconstrained qubits have a state-counting term of $N_A \log(2)$. Adding $N_A \log(2)$ to Eq. (A25) yields the noncommuting-charge state-counting term:

$$\begin{aligned} S(\langle \rho_A \rangle_{\mathcal{N}_0}) &= N_A \log(2) - \sum_{s_A=0}^{\frac{N_A}{2}} \left(\frac{N}{2} + 1 \right) \frac{(\frac{N}{2})! (\frac{N}{2})!}{N!} \binom{2s_A + 1}{\frac{N_A}{2} + s_A + 1} \binom{2s_A + 1}{\frac{N_B}{2} + s_A + 1} \binom{N_A}{\frac{N_A}{2} - s_A} \binom{N_B}{\frac{N_B}{2} - s_A} \\ &\quad \times \log \left(\frac{(\frac{N}{2})! (\frac{N}{2})!}{N!} \frac{(\frac{N}{2} + 1)}{(\frac{N_B}{2} + s_A + 1)} \binom{N_B}{\frac{N_B}{2} - s_A} \right). \end{aligned} \quad (\text{A26})$$

A 3 ii Closed-form approximation to the noncommuting-charge model's state-counting term

First, we approximate the $\frac{d_A d_B}{D}$ in Eq. (A24) as a Gaussian function. We break $\frac{d_A d_B}{D}$ into two factors, one consisting of factorials and the other of everything else: $\frac{d_A d_B}{D} = f(s_A)g(s_A)$, wherein

$$f(s_A) := \frac{(\frac{N}{2})! (\frac{N}{2})!}{(N)!} \frac{(N_A)!}{(\frac{N_A}{2} + s_A)! (\frac{N_A}{2} - s_A)!} \frac{(N_B)!}{(\frac{N_B}{2} + s_B)! (\frac{N_B}{2} - s_B)!} \quad \text{and} \quad (\text{A27})$$

$$g(s_A) := \binom{2s_A + 1}{\frac{N_A}{2} + s_A + 1} \binom{2s_A + 1}{\frac{N_B}{2} + s_A + 1} \left(\frac{N}{2} + 1 \right). \quad (\text{A28})$$

We Taylor-expand $\log(f(s_A))$ around its maximum, $s_A = 0$, to $\mathcal{O}(N^{-1})$, assuming $s_A^2 \sim N$. Then, we exponentiate the result:

$$f(s_A) = \sqrt{\frac{2N}{N_A N_B \pi}} \exp \left(\frac{-2N s_A^2}{N_A N_B} \right) \left[1 + \frac{1}{4N} - \frac{1}{4N_A} - \frac{1}{4N_B} + \frac{2s_A^2}{N_A^2} + \frac{2s_A^2}{N_B^2} - \frac{4s_A^4}{3N_A^3} - \frac{4s_A^4}{3N_B^3} + \mathcal{O}(N^{-2}) \right]. \quad (\text{A29})$$

Next, we expand $g(s_A)$ [Eq. (A28)]:

$$g(s_A) = \frac{8N s_A^2}{N_A N_B} \left[1 + \frac{1}{s_A} - \frac{2s_A}{N_A} - \frac{2s_A}{N_B} + \frac{2}{N} - \frac{4}{N_A} - \frac{4}{N_B} + \frac{1}{4s_A^2} + \frac{4s_A^2}{N_A^2} + \frac{4s_A^2}{N_B^2} + \frac{4s_A^2}{N_A N_B} + \mathcal{O}(N^{-3/2}) \right]. \quad (\text{A30})$$

The right-hand sides of (A29) and (A30) multiply to

$$\begin{aligned} \frac{d_A d_B}{D} &= \frac{4(2N)^{\frac{3}{2}}}{(N_A N_B)^{\frac{3}{2}} \sqrt{\pi}} s_A^2 \exp \left(\frac{-2N s_A^2}{N_A N_B} \right) \left[1 + \frac{1}{s_A} - \frac{2N s_A}{N_A N_B} + \frac{9}{4N} - \frac{17N}{4N_A N_B} + \frac{6s_A^2}{N_A^2} + \frac{6s_A^2}{N_B^2} + \frac{4s_A^2}{N_A N_B} \right. \\ &\quad \left. + \frac{1}{4s_A^2} - \frac{4s_A^4}{3N_A^3} - \frac{4s_A^4}{3N_B^3} + \mathcal{O}(N^{-3/2}) \right]. \end{aligned} \quad (\text{A31})$$

We check that this function is normalized, as $\frac{d_A d_B}{D}$ must be, but omit the details of the check.

Having approximated the first factor in the state-counting term (A24), we proceed to the second. According to the Stirling approximation (A14), the logarithm is

$$\begin{aligned} \log\left(\frac{d_B}{D(2s_A+1)}\right) &= -N \log(2) + \frac{N_B}{2} \log\left(\frac{N_B^2}{\left(\frac{N_B}{2}-s_A\right)\left(\frac{N_B}{2}+s_A\right)}\right) + s_A \log\left(\frac{\frac{N_B}{2}-s_A}{\frac{N_B}{2}+s_A}\right) \\ &\quad + \frac{1}{2} \log\left(\frac{NN_B}{4\left(\frac{N_B}{2}-s_A\right)\left(\frac{N_B}{2}+s_A\right)}\right) + \log\left(\frac{\frac{N}{2}+1}{\frac{N_B}{2}+s_A+1}\right) \\ &\quad + \frac{1}{4N} + \frac{1}{12N_B} - \frac{1}{12\left(\frac{N_B}{2}-s_A\right)} - \frac{1}{12\left(\frac{N_B}{2}+s_A\right)} + \mathcal{O}(N^{-2}). \end{aligned} \quad (\text{A32})$$

Taylor-approximating about $N = \infty$ yields

$$\log\left(\frac{d_B}{D(2s_A+1)}\right) = -N_A \log(2) + \frac{3}{2} \log\left(\frac{N}{N_B}\right) - \frac{2s_A^2}{N_B} - \frac{2s_A}{N_B} - \frac{4s_A^4}{3N_B^3} + \frac{4s_A^2}{N_B^2} + \frac{9}{4N} - \frac{9}{4N_B} + \mathcal{O}(N^{-3/2}). \quad (\text{A33})$$

We can now substitute the logarithm (A33) and the $d_A d_B / D$ factor (A31) into the state-counting term (A24). Since the summand varies slowly where its value is large, we approximate the sum as an integral. Also, since the integrand falls off rapidly at large s_A , we approximate the integral's upper limit with ∞ . Evaluating the integral, we estimate the a qubits' contribution to the state-counting term. Adding the b qubits' state-counting term, $N_A \log(2)$, we obtain the noncommuting-charge state-counting term:

$$\langle S_E \rangle_S = N_A \log(4) - \frac{3}{2} \log\left(\frac{N}{N_B}\right) + \frac{3N_A}{2N} + \frac{3N_A}{4N^2} + \frac{N_A^2}{2N^2 N_B} + \mathcal{O}(N^{-3/2}). \quad (\text{A34})$$

Appendix B HOW OUR MODELS' CHARGES RESTRICT THE MICROCANONICAL SUBSPACES

The main text posits an explanation for why, in the microcanonical-subspace study, the noncommuting-charge Page curve lies above the commuting-charge Page curve. We propose another explanation, using specifics of our models, here. To what extent this reasoning generalizes beyond those models merits further study.

Consider beginning with an unconstrained system, then restricting the Hilbert space to the eigenvalue-0 eigenspace of Q_1^{tot} , then restricting further to the eigenvalue-0 eigenspace of Q_2^{tot} , then restricting to the eigenvalue-0 eigenspace of Q_3^{tot} . The first two restrictions already restrict the system to the $s = 0$ subspace; the third restriction is redundant.

Now, consider undertaking the same process but replacing the Q_α^{tot} 's with C_α^{tot} 's. The first two restrictions only partially imply the third, which therefore constrains the Hilbert space nontrivially. (Appendix B 1 contains a proof.) One might therefore expect the microcanonical subspace to be larger when defined by our three noncommuting charges than when defined by our three commuting charges. We have confirmed this expectation by direct calculation. Furthermore, the available Hilbert space's dimensionality upper-bounds the entanglement entropy [Eq. (1)]. Hence the noncommuting charges should enable more entanglement—a higher Page curve—than the commuting charges do.

B 1 Constraining C_1^{tot} and C_2^{tot} constrains C_3^{tot} only partially

Consider an unconstrained system of N 4-level qudits. Consider restricting the Hilbert space to the eigenvalue-0 eigenspace of C_1^{tot} , then restricting further to the eigenvalue-0 eigenspace of C_2^{tot} , and then restricting to the eigenvalue-0 eigenspace of C_3^{tot} . The first two restrictions partially imply the third, which constrains the Hilbert space nontrivially.

The local charges $C_{1,2,3}$ share four eigenstates, the maximally entangled Bell states [102]. They are, if $|\uparrow\rangle$ and $|\downarrow\rangle$ denote the Z eigenstates,

$$|\text{B}_1\rangle := \frac{1}{\sqrt{2}} (|\downarrow\rangle_a |\uparrow\rangle_b - |\uparrow\rangle_a |\downarrow\rangle_b), \quad |\text{B}_2\rangle := \frac{1}{\sqrt{2}} (|\downarrow\rangle_a |\downarrow\rangle_b - |\uparrow\rangle_a |\uparrow\rangle_b), \quad (\text{B1})$$

$$|\text{B}_3\rangle := \frac{1}{\sqrt{2}} (|\downarrow\rangle_a |\downarrow\rangle_b + |\uparrow\rangle_a |\uparrow\rangle_b), \quad \text{and} \quad |\text{B}_4\rangle := \frac{1}{\sqrt{2}} (|\downarrow\rangle_a |\uparrow\rangle_b + |\uparrow\rangle_a |\downarrow\rangle_b). \quad (\text{B2})$$

Denote by ρ_j the j^{th} qubit's reduced state, which has a weight $\langle \text{B}_k | \rho_j | \text{B}_k \rangle$ on the k^{th} Bell state. Summing over qudits yields the total population $P_k := \sum_{j=1}^N \langle \text{B}_k | \rho_j | \text{B}_k \rangle$.

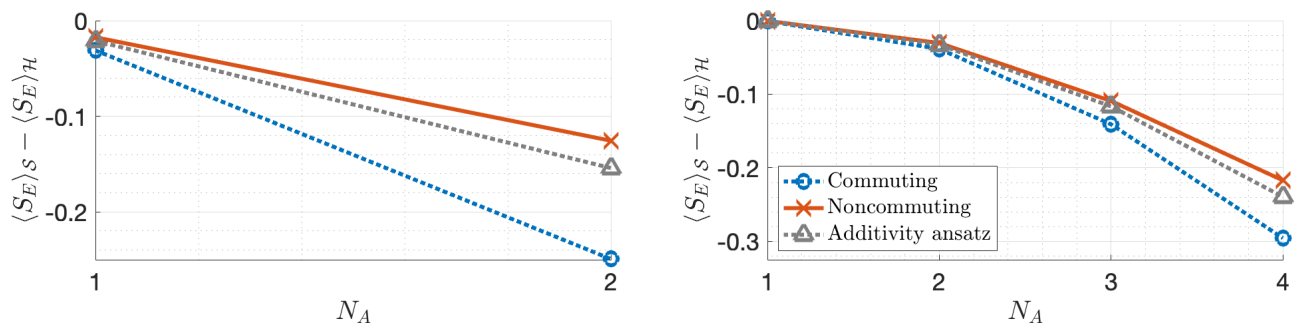


Figure 3: Testing the additivity ansatz. $\langle S_E \rangle_S$ denote any Page curve restricted by charges; and $\langle S_E \rangle_{\mathcal{H}}$, the unrestricted Page curve. The red x's form the noncommuting-charge model's Page curve, and the circular blue markers form the commuting-charge model's Page curve. Both curves were calculated using microcanonical subspaces. The gray triangles illustrate the additivity ansatz.

If the system is in an eigenvalue-0 eigenstate of C_1^{tot} , then $P_1 + P_2 = P_3 + P_4$. If the system is in an eigenvalue-0 eigenstate of C_2^{tot} , then $P_1 + P_3 = P_2 + P_4$. Together, these constraints imply $P_1 = P_4$ and $P_2 = P_3$. Furthermore, $\langle C_3^{\text{tot}} \rangle = P_2 + P_3 - P_1 - P_4$. This expectation value, under the $C_{1,2}^{\text{tot}}$ constraints, is restricted to $2(P_2 - P_1)$, which need not vanish. Thus, the first two charges do not restrict the C_3^{tot} expectation value completely. Contrarily, if in an eigenstate of $Q_{1,2}^{\text{tot}}$, the system is in the eigenvalue-0 eigenstate of Q_3^{tot} . Hence $C_{1,2}^{\text{tot}}$ restrict the Hilbert space less than $Q_{1,2}^{\text{tot}}$ do.

Appendix C EXTENT TO WHICH CHARGES CONSTRAIN THE PAGE CURVE ADDITIVELY

Figure 2 shows Page curves constructed from microcanonical subspaces. At finite N , the curves violate an expectation that one might gather from earlier literature. We explain the expectation, discuss the violation, and provide numerical evidence for the expectation in the thermodynamic limit (as $N \rightarrow \infty$).

Consider beginning with an unconstrained N -site system, restricting the Hilbert space to the eigenvalue-0 eigenspace of C_1^{tot} , then restricting further to the eigenvalue-0 eigenspace of C_2^{tot} , and then restricting to the eigenvalue-0 eigenspace of C_3^{tot} . One might expect that, as more charges were introduced, each successive charge would lower the Page curve by the same amount as the last charge. Such lowering has been argued to happen in the thermodynamic limit [15]. We call an expectation of such lowering the *additivity ansatz*. One might posit it (i) for noncommuting charges in the thermodynamic limit and (ii) for commuting and noncommuting charges at finite N .

If the additivity ansatz were true, the Page curve (for three equivalent commuting or noncommuting charges) could be constructed as follows. Consider restricting the global Hilbert space to one charge's eigenvalue-0 eigenspace (any C_α^{tot} or Q_α^{tot} —which one does not affect the curve). The corresponding Page curve, we denote by $\langle S_E \rangle_S^{(1)}$. Recall that $\langle S_E \rangle_{\mathcal{H}}$ denotes the unrestricted Page curve. The additivity ansatz predicts the Page curve $\langle S_E \rangle_{\mathcal{H}} - 3 \left(\langle S_E \rangle_{\mathcal{H}} - \langle S_E \rangle_S^{(1)} \right)$ for our models with three equivalent charges constrained in each.

Figure 3 tests this prediction at finite N . The gray triangles form the additivity-ansatz curve. It lies below the noncommuting-charge Page curve (red x's), which are therefore superadditive. The ansatz curve also lies above the commuting-charge Page curve (blue circles), which are subadditive. Hence the additivity ansatz breaks in a commutation-dependent manner at finite N . However, all three curves converge as N grows. We hence provide numerical evidence for the additivity ansatz, supported analytically in [15] and in App. A above, in the thermodynamic limit.

Appendix D ANALOGOUS APPROXIMATE MICROCANONICAL SUBSPACES

The main text specifies how to construct AMC subspaces in the noncommuting-charge model. We augment this explanation with examples. Then, we explain how to construct analogous AMC subspaces in the commuting-charge model. We also specify the six analogous-AMC-subspace pairs reported in the main text.

First, we review how to construct AMC subspaces in the noncommuting-charge model. Denote by m the Z_a^{tot} eigenvalue. Z_a^{tot} shares eigenstates with \vec{S}_a^2 . Shared eigenstates labeled by the same two quantum numbers form the

(s, m)	Possible measurement outcomes								
	-4	-3	-2	-1	0	1	2	3	4
(1, 0)			0.500	0	0.500				
(1, 1)			0.250	0.500	0.250				
(2, 0)		0.375	0	0.250	0	0.375			
(2, 1)		0.250	0.250	0	0.250	0.250			
(2, 2)		0.063	0.250	0.375	0.250	0.063			
(3, 0)	0.313	0	0.188	0	0.188	0	0.313		
(3, 1)	0.234	0.156	0.016	0.188	0.016	0.156	0.234		
(3, 2)	0.094	0.250	0.156	0	0.156	0.250	0.094		
(3, 3)	0.016	0.094	0.234	0.313	0.234	0.094	0.016		
(4, 0)	0.273	0	0.156	0	0.141	0	0.156	0	0.273
(4, 1)	0.219	0.109	0.031	0.141	0	0.141	0.031	0.109	0.219
(4, 2)	0.109	0.219	0.063	0.031	0.156	0.031	0.063	0.219	0.109
(4, 3)	0.031	0.141	0.219	0.109	0	0.109	0.219	0.141	0.031
(4, 4)	0.004	0.031	0.109	0.219	0.273	0.219	0.109	0.031	0.004

Table I: Probabilities $p_1^N(\gamma)$ that characterize (s, m) eigenspaces. Denote by $|\psi\rangle$ any state from an (s, m) eigenspace of the noncommuting-charge model. Measuring Q_1^{tot} yields outcome γ with some probability. This probability, averaged over the $|\psi\rangle$, we denote by $p_1^N(\gamma)$. The possible measurement outcomes range from $-s$ to s . The probabilities $p_1^N(\gamma)$ are listed for each (s, m) and are independent of the system size, N . $p_1^N(\gamma)$ has exactly one peak only if $s = m$.

(s, m) eigenspace. Some such eigenspaces are AMC subspaces, we find by direct calculation. For each (s, m) value, we calculate the probability distributions $p_\alpha^N(\gamma)$. Each distribution must exhibit one peak for the eigenspace to satisfy the AMC subspace's definition. $p_3^N(\gamma)$, being a Kronecker delta function in the (s, m) subspace, meets this criterion. Also, according to direct calculation, $p_1^N(\gamma) = p_2^N(\gamma)$ for all γ . Hence we need calculate only $p_1^N(\gamma)$ to check whether an (s, m) eigenspace is an AMC subspace. Table I presents these distributions for $s \leq 4$. Whenever $s = m$, each distribution exhibits one peak. Therefore, each $(s, m=s)$ subspace qualifies as an AMC subspace.

Having identified AMC subspaces defined by noncommuting charges, we construct analogs defined by commuting charges. For each N , we identify the eigenspaces shared by $C_{1,2,3}^{\text{tot}}$. For consistency with the noncommuting-charge model, we keep only the eigenvalue- m eigenspaces of C_3^{tot} . For each shared eigenspace, we calculate the distributions $p_\alpha^C(\gamma)$. If they equal their noncommuting-charge counterparts $p_\alpha^N(\gamma)$ (criterion 5), the eigenspace forms an analogous AMC subspace.

An illustrative example is parameterized by $N = 8$ and (in the noncommuting-charge model) $s = m = 1$. We keep only the eigenvalue-1 eigenspaces of C_3^{tot} . Denote by c_x the C_1^{tot} eigenvalues and by c_y the C_2^{tot} eigenvalues. We label by $(c_x, c_y, 1)$ the eigenspaces shared by $C_{1,2,3}^{\text{tot}}$. For consistency with the noncommuting-charge model, we ignore any eigenspaces in which $c_x > s$ or $c_y > s$. Four eigenspaces remain: $(0, -1, 1)$, $(-1, 0, 1)$, $(1, 0, 1)$, and $(0, 1, 1)$. Each is of dimension 1680. The candidate AMC subspace is the union of these four subspaces and is of dimension 6720. All these dimensions fix the probabilities $p_1^C(\gamma)$. For example, $p_1^C(0) = (1680 \times 2)/6720 = 0.5$. The remaining probabilities are $p_1^C(-1) = 0.25$ and $p_1^C(1) = 0.25$. This distribution equals the corresponding $p_1^N(\gamma)$. Checking every eigenvalue- m eigenspace of C_3^{tot} , we find six eigenspaces for which $p_\alpha^C(\gamma) = p_\alpha^N(\gamma) \forall \alpha, \gamma$, satisfying criterion 5.

We have identified six pairs of parallel (commuting-charge and noncommuting-charge) AMC subspaces. The pairs are labeled by $s = m = 1, N/2$ and $N = 4, 8$, as well as by $s = m = N/2$ and $N = 2, 6$. (Computational limitations restrict us to $N \leq 8$.) Table II compares the two Page curves formed from each subspace pair. We compare the curves at their midpoints, $N_A = N/2$. The percent difference between the two curves varies from 0.199% to 3.06% across the subspace pairs. Hence noncommuting charges increase the average entanglement entropy in AMC subspaces as in microcanonical subspaces.

REFERENCES

- [1] M. Van Raamsdonk, Building up space-time with quantum entanglement, International Journal of Modern Physics D **19**, 2429 (2010).
- [2] B. Swingle, Spacetime from entanglement, Annual Review of Condensed Matter Physics **9**, 345 (2018).
- [3] C. Cao, S. M. Carroll, and S. Michalakis, Space from hilbert space: recovering geometry from bulk entanglement, Physical Review D **95**, 024031 (2017).
- [4] B. Skinner, J. Ruhman, and A. Nahum, Measurement-induced phase transitions in the dynamics of entanglement, Physical Review X **9**, 031009 (2019).

N	$s = m$	NC	C	NC - C	% diff.
4	1	-0.455	-0.479	0.024	5.112
8	1	-0.364	-0.390	0.027	7.106
2	$N/2$	-0.587	-0.589	0.002	0.362
4	$N/2$	-1.350	-1.354	0.004	0.272
6	$N/2$	-2.074	-2.086	0.012	0.600
8	$N/2$	-2.770	-2.788	0.017	0.625

Table II: Differences between Page curves, constructed from approximate microcanonical subspaces, at $N_A = N/2$. The Page curves' values at $N_A = N/2$ are listed for various N and $s = m$ values. We abbreviate “difference” with “diff.,” “noncommuting” with “NC,” and “commuting” with “C.”

- [5] Y. Li, X. Chen, and M. P. Fisher, Measurement-driven entanglement transition in hybrid quantum circuits, *Physical Review B* **100**, 134306 (2019).
- [6] A. Chan, R. M. Nandkishore, M. Pretko, and G. Smith, Unitary-projective entanglement dynamics, *Phys. Rev. B* **99**, 224307 (2019).
- [7] R. Somma, G. Ortiz, H. Barnum, E. Knill, and L. Viola, Nature and measure of entanglement in quantum phase transitions, *Physical Review A* **70**, 042311 (2004).
- [8] S. D. Geraedts, N. Regnault, and R. M. Nandkishore, Characterizing the many-body localization transition using the entanglement spectrum, *New Journal of Physics* **19**, 113021 (2017).
- [9] Y. Bao, S. Choi, and E. Altman, Theory of the phase transition in random unitary circuits with measurements, *Physical Review B* **101**, 104301 (2020).
- [10] M. J. Gullans and D. A. Huse, Dynamical purification phase transition induced by quantum measurements, *Physical Review X* **10**, 041020 (2020).
- [11] X.-G. Wen, Choreographed entanglement dances: Topological states of quantum matter, *Science* **363**, eaal3099 (2019).
- [12] B. Zeng, X. Chen, D.-L. Zhou, and X.-G. Wen, Quantum information meets quantum matter—from quantum entanglement to topological phase in many-body systems, *arXiv:1508.02595* (2015).
- [13] D. A. Abanin, E. Altman, I. Bloch, and M. Serbyn, Colloquium: Many-body localization, thermalization, and entanglement, *Reviews of Modern Physics* **91**, 021001 (2019).
- [14] D. N. Page, Average entropy of a subsystem, *Physical review letters* **71**, 1291 (1993).
- [15] A. Altland, D. A. Huse, and T. Micklitz, Maximum entropy quantum state distributions, *arXiv:2203.12580* (2022).
- [16] F. Monteiro, M. Tezuka, A. Altland, D. A. Huse, and T. Micklitz, Quantum ergodicity in the many-body localization problem, *Physical Review Letters* **127**, 030601 (2021).
- [17] Y. O. Nakagawa, M. Watanabe, H. Fujita, and S. Sugiura, Universality in volume-law entanglement of scrambled pure quantum states, *Nature communications* **9**, 1 (2018).
- [18] L. Hackl, L. Vidmar, M. Rigol, and E. Bianchi, Average eigenstate entanglement entropy of the xy chain in a transverse field and its universality for translationally invariant quadratic fermionic models, *Physical Review B* **99**, 075123 (2019).
- [19] L. Hackl and E. Bianchi, Bosonic and fermionic gaussian states from kähler structures, *SciPost Physics Core* **4**, 025 (2021).
- [20] L. Vidmar and M. Rigol, Entanglement entropy of eigenstates of quantum chaotic hamiltonians, *Physical review letters* **119**, 220603 (2017).
- [21] E. Bianchi and P. Dona, Typical entanglement entropy in the presence of a center: Page curve and its variance, *Physical Review D* **100**, 105010 (2019).
- [22] E. Bianchi, L. Hackl, M. Kieburg, M. Rigol, and L. Vidmar, Volume-law entanglement entropy of typical pure quantum states, *arXiv:2112.06959* (2021).
- [23] S. Murciano, P. Calabrese, and L. Piroli, Symmetry-resolved page curves, *arXiv:2206.05083* (2022).
- [24] M. Goldstein and E. Sela, Symmetry-resolved entanglement in many-body systems, *Physical review letters* **120**, 200602 (2018).
- [25] J. Xavier, F. Alcaraz, and G. Sierra, Equipartition of the entanglement entropy, *Physical Review B* **98**, 041106 (2018).
- [26] P. Calabrese, J. Dubail, and S. Murciano, Symmetry-resolved entanglement entropy in wess-zumino-witten models, *Journal of High Energy Physics* **2021**, 1 (2021).
- [27] N. Laflorencie and S. Rachel, Spin-resolved entanglement spectroscopy of critical spin chains and luttinger liquids, *Journal of Statistical Mechanics: Theory and Experiment* **2014**, P11013 (2014).
- [28] R. Bonsignori, P. Ruggiero, and P. Calabrese, Symmetry resolved entanglement in free fermionic systems, *Journal of Physics A: Mathematical and Theoretical* **52**, 475302 (2019).
- [29] A. Belin, L.-Y. Hung, A. Maloney, S. Matsuura, R. C. Myers, and T. Sierens, Holographic charged rényi entropies, *Journal of High Energy Physics* **2013**, 1 (2013).
- [30] E. Cornfeld, M. Goldstein, and E. Sela, Imbalance entanglement: Symmetry decomposition of negativity, *Physical Review A* **98**, 032302 (2018).
- [31] H. Barghathi, C. Herdman, and A. Del Maestro, Rényi generalization of the accessible entanglement entropy, *Physical Review Letters* **121**, 150501 (2018).

- [32] M. T. Tan and S. Ryu, Particle number fluctuations, rényi entropy, and symmetry-resolved entanglement entropy in a two-dimensional fermi gas from multidimensional bosonization, *Physical Review B* **101**, 235169 (2020).
- [33] S. Murciano, P. Ruggiero, and P. Calabrese, Symmetry resolved entanglement in two-dimensional systems via dimensional reduction, *Journal of Statistical Mechanics: Theory and Experiment* **2020**, 083102 (2020).
- [34] M. Kiefer-Emmanouilidis, R. Unanyan, M. Fleischhauer, and J. Sirker, Evidence for unbounded growth of the number entropy in many-body localized phases, *Physical Review Letters* **124**, 243601 (2020).
- [35] D. Grimmer, B. de SL Torres, and E. Martín-Martínez, Measurements in qft: Weakly coupled local particle detectors and entanglement harvesting, *Physical Review D* **104**, 085014 (2021).
- [36] R. Haag, *Local quantum physics: Fields, particles, algebras* (Springer Science & Business Media, 2012).
- [37] R. Balian and N. Balazs, Equiprobability, inference, and entropy in quantum theory, *Annals of Physics* **179**, 97 (1987).
- [38] E. T. Jaynes, Information theory and statistical mechanics. ii, *Physical review* **108**, 171 (1957).
- [39] M. Lostaglio, *The resource theory of quantum thermodynamics*, Master's thesis, Imperial College London (2014).
- [40] N. Yunger Halpern, Beyond heat baths ii: framework for generalized thermodynamic resource theories, *Journal of Physics A: Mathematical and Theoretical* **51**, 094001 (2018).
- [41] C. Murthy, A. Babakhani, F. Iniguez, M. Srednicki, and N. Y. Halpern, Non-abelian eigenstate thermalization hypothesis, arXiv:2206.05310 (2022).
- [42] N. Yunger Halpern, P. Faist, J. Oppenheim, and A. Winter, Microcanonical and resource-theoretic derivations of the thermal state of a quantum system with noncommuting charges, *Nat. Commun.* **7**, 12051 (2016).
- [43] Y. Guryanova, S. Popescu, A. J. Short, R. Silva, and P. Skrzypczyk, Thermodynamics of quantum systems with multiple conserved quantities, *Nat. Commun.* **7**, 12049 (2016).
- [44] M. Lostaglio, D. Jennings, and T. Rudolph, Thermodynamic resource theories, non-commutativity and maximum entropy principles, *New J. Phys.* **19**, 043008 (2017).
- [45] C. Sparaciari, L. Del Rio, C. M. Scandolo, P. Faist, and J. Oppenheim, The first law of general quantum resource theories, *Quantum* **4**, 259 (2020).
- [46] Z. B. Khanian, From quantum source compression to quantum thermodynamics, arXiv:2012.14143 (2020).
- [47] Z. B. Khanian, M. N. Bera, A. Riera, M. Lewenstein, and A. Winter, Resource theory of heat and work with non-commuting charges: yet another new foundation of thermodynamics, arXiv:2011.08020 (2020).
- [48] G. Manzano, J. M. Parrondo, and G. T. Landi, Non-abelian quantum transport and thermosqueezing effects, *PRX Quantum* **3**, 010304 (2022).
- [49] N. Yunger Halpern and S. Majidy, How to build hamiltonians that transport noncommuting charges in quantum thermodynamics, *npj Quantum Information* **8**, 1 (2022).
- [50] F. Kranzl, A. Lasek, M. K. Joshi, A. Kalev, R. Blatt, C. F. Roos, and N. Y. Halpern, Experimental observation of thermalisation with noncommuting charges, arXiv:2202.04652 (2022).
- [51] J. A. Vaccaro and S. M. Barnett, Information erasure without an energy cost, *Proc. Math. Phys. Eng. Sci.* **467**, 1770 (2011).
- [52] G. Gour, D. Jennings, F. Buscemi, R. Duan, and I. Marvian, Quantum majorization and a complete set of entropic conditions for quantum thermodynamics, *Nat. Commun.* **9**, 5352 (2018).
- [53] S. Popescu, A. B. Sainz, A. J. Short, and A. Winter, Quantum reference frames and their applications to thermodynamics, *Philos. Trans. Royal Soc. A* **376**, 20180111 (2018).
- [54] S. Popescu, A. B. Sainz, A. J. Short, and A. Winter, Reference frames which separately store noncommuting conserved quantities, *Phys. Rev. Lett.* **125**, 090601 (2020).
- [55] K. Ito and M. Hayashi, Optimal performance of generalized heat engines with finite-size baths of arbitrary multiple conserved quantities beyond independent-and-identical-distribution scaling, *Phys. Rev. E* **97**, 012129 (2018).
- [56] M. N. Bera, A. Riera, M. Lewenstein, Z. B. Khanian, and A. Winter, Thermodynamics as a consequence of information conservation, *Quantum* **3**, 121 (2019).
- [57] J. Mur-Petit, A. Relaño, R. Molina, and D. Jaksch, Revealing missing charges with generalised quantum fluctuation relations, *Nature communications* **9**, 1 (2018).
- [58] G. Manzano, Squeezed thermal reservoir as a generalized equilibrium reservoir, *Phys. Rev. E* **98**, 042123 (2018).
- [59] N. Yunger Halpern, M. E. Beverland, and A. Kalev, Noncommuting conserved charges in quantum many-body thermalization, *Phys. Rev. E* **101**, 042117 (2020).
- [60] G. Manzano, R. Sánchez, R. Silva, G. Haack, J. B. Brask, N. Brunner, and P. P. Potts, Hybrid thermal machines: Generalized thermodynamic resources for multitasking, *Phys. Rev. Res.* **2**, 043302 (2020).
- [61] K. Fukai, Y. Nozawa, K. Kawahara, and T. N. Ikeda, Noncommutative generalized gibbs ensemble in isolated integrable quantum systems, *Phys. Rev. Res.* **2**, 033403 (2020).
- [62] M. Scandi and M. Perarnau-Llobet, Thermodynamic length in open quantum systems, *Quantum* **3**, 197 (2019).
- [63] P. Boes, H. Wilming, J. Eisert, and R. Gallego, Statistical ensembles without typicality, *Nat. Commun.* **9**, 1 (2018).
- [64] Y. Mitsuhashi, K. Kaneko, and T. Sagawa, Characterizing symmetry-protected thermal equilibrium by work extraction, arXiv:2103.06060 (2021).
- [65] T. Croucher, J. Wright, A. R. R. Carvalho, S. M. Barnett, and J. A. Vaccaro, Information erasure, in *Thermodynamics in the Quantum Regime: Fundamental Aspects and New Directions*, edited by F. Binder, L. A. Correa, C. Gogolin, J. Anders, and G. Adesso (Springer International Publishing, Cham, 2018) pp. 713–730.
- [66] J. S. S. T. Wright, T. Gould, A. R. R. Carvalho, S. Bedkihal, and J. A. Vaccaro, Quantum heat engine operating between thermal and spin reservoirs, *Phys. Rev. A* **97**, 052104 (2018).
- [67] Z. Zhang, J. Tindall, J. Mur-Petit, D. Jaksch, and B. Buča, Stationary state degeneracy of open quantum systems with

- non-abelian symmetries, *Journal of Physics A* **53**, 215304 (2020).
- [68] M. Medenjak, B. Buča, and D. Jaksch, Isolated heisenberg magnet as a quantum time crystal, *Phys. Rev. B* **102**, 041117 (2020).
- [69] T. Croucher and J. A. Vaccaro, Memory erasure with finite-sized spin reservoir, arXiv:2111.10930 (2021).
- [70] I. Marvian, H. Liu, and A. Hulse, Qudit circuits with $SU(d)$ symmetry: Locality imposes additional conservation laws, arXiv:2105.12877 (2021).
- [71] I. Marvian, H. Liu, and A. Hulse, Rotationally-Invariant Circuits: Universality with the exchange interaction and two ancilla qubits, arXiv:2202.01963 (2022).
- [72] A. F. Ducuara, *Quantum Resource Theories: Operational Tasks and Information-Theoretic Quantities*, Ph.D. thesis, U. of Bristol (2022).
- [73] E. Hinds Mingo, Y. Guryanova, P. Faist, and D. Jennings, Quantum thermodynamics with multiple conserved quantities, in *Thermodynamics in the Quantum Regime* (Springer, 2018) pp. 751–771.
- [74] I. Marvian, Restrictions on realizable unitary operations imposed by symmetry and locality, *Nature Physics* **18**, 283 (2022).
- [75] J. Mur-Petit, A. Relaño, R. A. Molina, and D. Jaksch, Fluctuations of work in realistic equilibrium states of quantum systems with conserved quantities, *SciPost Physics Proceedings*, 024 (2020).
- [76] P. Strasberg, A. Winter, J. Gemmer, and J. Wang, Classicality, markovianity and local detailed balance from pure state dynamics, arXiv:2209.07977 (2022).
- [77] M. A. Nielsen and I. Chuang, *Quantum computation and quantum information* (2002).
- [78] PennyLane, Understanding the Haar measure, https://pennylane.ai/qml/demos/tutorial_haar_measure.html (2021).
- [79] Computational restrictions prevent $N_B - N_A$ from growing very large in the numerics. Therefore, we refrain from plotting our analytics in Fig. 2.
- [80] In both expressions, the $\mathcal{O}(N^{-\frac{3}{2}})$ term may vanish, so the next nonzero term may be $\mathcal{O}(N^{-2})$.
- [81] R. Shankar, *Principles of quantum mechanics* (Springer Science & Business Media, 2012).
- [82] Y. Ogata, Approximating macroscopic observables in quantum spin systems with commuting matrices, *Journal of Functional Analysis* **264**, 2005 (2013).
- [83] H.-J. Stöckmann, *Quantum chaos: an introduction* (2000).
- [84] L. D’Alessio, Y. Kafri, A. Polkovnikov, and M. Rigol, From quantum chaos and eigenstate thermalization to statistical mechanics and thermodynamics, *Adv. Phys.* **65**, 239 (2016), <https://doi.org/10.1080/00018732.2016.1198134>.
- [85] K. Hashimoto, K. Murata, and R. Yoshii, Out-of-time-order correlators in quantum mechanics, *Journal of High Energy Physics* **2017**, 1 (2017).
- [86] E. B. Rozenbaum, S. Ganeshan, and V. Galitski, Lyapunov exponent and out-of-time-ordered correlator’s growth rate in a chaotic system, *Physical review letters* **118**, 086801 (2017).
- [87] I. García-Mata, M. Saraceno, R. A. Jalabert, A. J. Roncaglia, and D. A. Wisniacki, Chaos signatures in the short and long time behavior of the out-of-time ordered correlator, *Physical review letters* **121**, 210601 (2018).
- [88] J. R. G. Alonso, N. Shammah, S. Ahmed, F. Nori, and J. Dressel, Diagnosing quantum chaos with out-of-time-ordered-correlator quasiprobability in the kicked-top model, arXiv:2201.08175 (2022).
- [89] M. Fisher, V. Khemani, A. Nahum, and S. Vijay, Random quantum circuits, arXiv:2207.14280 (2022).
- [90] A. Hulse, H. Liu, and I. Marvian, Qudit circuits with $su(d)$ symmetry: Locality imposes additional conservation laws, arXiv:2105.12877 (2021).
- [91] I. Buluta and F. Nori, Quantum simulators, *Science* **326**, 108 (2009).
- [92] J. Biamonte, P. Wittek, N. Pancotti, P. Rebentrost, N. Wiebe, and S. Lloyd, Quantum machine learning, *Nature* **549**, 195 (2017).
- [93] A. C. Potter and R. Vasseur, Symmetry constraints on many-body localization, *Physical Review B* **94**, 224206 (2016).
- [94] N. M. Linke, S. Johri, C. Figgatt, K. A. Landsman, A. Y. Matsuura, and C. Monroe, Measuring the rényi entropy of a two-site fermi-hubbard model on a trapped ion quantum computer, *Physical Review A* **98**, 052334 (2018).
- [95] R. Islam, R. Ma, P. M. Preiss, M. Eric Tai, A. Lukin, M. Rispoli, and M. Greiner, Measuring entanglement entropy in a quantum many-body system, *Nature* **528**, 77 (2015).
- [96] T. Brydges, A. Elben, P. Jurcevic, B. Vermersch, C. Maier, B. P. Lanyon, P. Zoller, R. Blatt, and C. F. Roos, Probing rényi entanglement entropy via randomized measurements, *Science* **364**, 260 (2019).
- [97] A. M. Kaufman, M. E. Tai, A. Lukin, M. Rispoli, R. Schittko, P. M. Preiss, and M. Greiner, Quantum thermalization through entanglement in an isolated many-body system, *Science* **353**, 794 (2016).
- [98] A. Lukin, M. Rispoli, R. Schittko, M. E. Tai, A. M. Kaufman, S. Choi, V. Khemani, J. Léonard, and M. Greiner, Probing entanglement in a many-body-localized system, *Science* **364**, 256 (2019).
- [99] J. Léonard, M. Rispoli, A. Lukin, R. Schittko, S. Kim, J. Kwan, D. Sels, E. Demler, and M. Greiner, Signatures of bath-induced quantum avalanches in a many-body-localized system, arXiv:2012.15270 (2020).
- [100] E. Cohen, T. Hansen, and N. Itzhaki, From entanglement witness to generalized catalan numbers, *Scientific Reports* **6**, 1 (2016).
- [101] R. P. Stanley, *Enumerative combinatorics volume 1 second edition*, Cambridge studies in advanced mathematics (2011).
- [102] M. A. Nielsen and I. L. Chuang, *Quantum Computation and Quantum Information* (Cambridge University Press, 2010).